Available online at www.sciencedirect.com
ScienceDirect
Journal of Sound and Vibration 315 (2008) 556–568
JOURNAL OF SOUND AND VIBRATION
www.elsevier.com/locate/jsvi

Basin boundaries in asymmetric vibrations of a circular plate

H.D. Park[a], W.K. Lee[b,*]

[a]RMS Technology Co., Ltd., Cheonan 330-174, Republic of Korea
[b]School of Mechanical Engineering, Yeungnam University, Gyongsan 712-749, Republic of Korea

Accepted 19 December 2007
The peer review of this article was organised by the Guest Editor
Available online 8 February 2008

Abstract

In order to investigate further nonlinear asymmetric vibrations of a clamped circular plate under a harmonic excitation, we reexamine a primary resonance, studied by Yeo and Lee [Corrected solvability conditions for non-linear asymmetric vibrations of a circular plate, *Journal of Sound and Vibration* 257 (2002) 653–665] in which at most three stable steady-state responses (one standing wave and two traveling waves) are observed to exist. Further examination, however, tells that there exist at most five stable steady-state responses: one standing wave and four traveling waves. Two of the traveling waves lose their stability by Hopf bifurcation and have a sequence of period-doubling bifurcations leading to chaos. When the system has five attractors: three equilibrium solutions (one standing wave and two traveling waves) and two chaotic attractors (two modulated traveling waves), the basin boundaries of the attractors on the principal plane are obtained. Also examined is how basin boundaries of the modulated motions (quasi-periodic and chaotic motions) evolve as a system parameter varies. The basin boundaries of the modulated motions turn out to have the fractal nature.

1. Introduction

Circular plates experience mid-plane stretching when deflected. The influence of this stretching on the dynamic response increases with the amplitude of the response. Then geometric nonlinearity due to the stretching should be included in the analysis. Using the dynamic analogue [1] of the von Kármán equations, Sridar et al. [2] studied nonlinear modal interactions of asymmetric vibrations of circular plates by deriving solvability conditions. Using these conditions they investigated the primary resonance (when excitation frequency is near the natural frequency of an asymmetric mode) to expect that the stable steady-state response is in the form of standing wave. Succeeding Sridar et al., Lee and his colleagues [3–8] have done a series of works on modal interaction of asymmetric vibrations of circular plates. Yeo and Lee [3] found that these conditions were misderived, and then corrected the conditions. They observed that in the primary resonance, the steady-state response could have not only the form of standing wave but also the form of traveling wave. Furthermore at most three stable steady-state responses (one standing wave and two traveling waves) were observed to exist. In case of internal resonance, in which the natural frequencies of two asymmetric modes are

*Corresponding author. Tel.: +82 53 810 2455.
E-mail addresses: parkhd@yumail.ac.kr (H.D. Park), wklee@yu.ac.kr (W.K. Lee).

0022-460X/$ - see front matter © 2007 Elsevier Ltd. All rights reserved.
doi:10.1016/j.jsv.2007.12.030

commensurable, Lee and Yeo [4] and Lee et al. [5] analyzed modal interactions of a clamped circular plate on an elastic foundation. For imperfect circular plates, Touzé et al. [9] and Thomas et al. [10] investigated the local bifurcations analytically and experimentally, respectively. Yeo and Lee [7] studied global bifurcations in modal interactions of a damped imperfect circular plate in order to find conditions under which Silnikov-type homoclinic orbit exists. Global bifurcations in modal interactions of an undamped imperfect circular plate were studied in terms of breaking of heteroclinic orbits and breaking of invariant tori by Samoylenko and Lee [8].

This study reexamines the primary resonance studied by Yeo and Lee [3] in order to investigate further nonlinear asymmetric vibrations of a perfect circular plate under a harmonic excitation. Further examination, however, tells that there exist at most five stable steady-state responses: one standing wave and four traveling waves. Two of the traveling waves lose their stability by Hopf bifurcation and have a sequence of period-doubling bifurcations leading to chaos. When the system has five attractors: three equilibrium solutions (one standing wave and two traveling waves) and two chaotic attractors (two modulated traveling waves), the basin boundaries of the attractors on the principal plane are obtained. Also examined is how basin boundaries of the modulated motions (quasi-periodic and chaotic motions) evolve as a system parameter varies. The basin boundaries of the modulated motions turn out to have the fractal nature.

2. Equations of motion

The equations governing the free, undamped oscillations of non-uniform circular plates were derived by Efstathiades [1]. These equations are simplified to fit the special case of uniform plates, and damping and forcing terms are added. Then the non-dimensionalized equations of motion of a circular plate shown in Fig. 1 are given as follows [2,11,12]:

$$\frac{\partial^2 w}{\partial t^2} + \nabla^4 w = \varepsilon\left[L(w,F) - 2c\frac{\partial w}{\partial t} + p(r,\theta,t)\right], \tag{1}$$

$$\nabla^4 F = \left(\frac{1}{r}\frac{\partial^2 w}{\partial r\partial\theta} - \frac{1}{r^2}\frac{\partial w}{\partial\theta}\right)^2 - \frac{\partial^2 w}{\partial r^2}\left(\frac{1}{r}\frac{\partial w}{\partial r} + \frac{1}{r^2}\frac{\partial^2 w}{\partial\theta^2}\right), \tag{2}$$

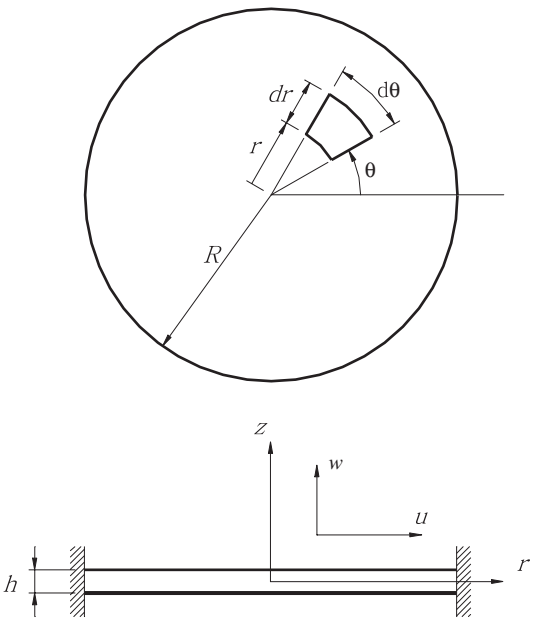

Fig. 1. A schematic diagram of a clamped circular plate.

where

$$L(w,F)=\frac{\partial^2 w}{\partial r^2}\left(\frac{1}{r}\frac{\partial F}{\partial r}+\frac{1}{r^2}\frac{\partial^2 F}{\partial\theta^2}\right)+\frac{\partial^2 F}{\partial r^2}\left(\frac{1}{r}\frac{\partial w}{\partial r}+\frac{1}{r^2}\frac{\partial^2 w}{\partial\theta^2}\right)-2\left(\frac{1}{r}\frac{\partial^2 F}{\partial r\partial\theta}-\frac{1}{r^2}\frac{\partial F}{\partial\theta}\right)\left(\frac{1}{r}\frac{\partial^2 w}{\partial r\partial\theta}-\frac{1}{r^2}\frac{\partial w}{\partial\theta}\right), \tag{3}$$

$$\nabla^4\equiv\left(\frac{\partial^2}{\partial r^2}+\frac{1}{r}\frac{\partial}{\partial r}+\frac{1}{r^2}\frac{\partial^2}{\partial\theta^2}\right)^2, \tag{4}$$

where $\varepsilon=12(1-\nu^2)h^2/R^2$ is a small parameter, ν is Poisson's ratio, h is the thickness, R is the radius, c is the damping coefficient, p is the forcing function, w is the deflection of middle surface, and F is the force function (stress function) satisfying compatibility condition.

The boundary conditions are developed for the plate, which is clamped along a circular edge. For all t and θ

$$w=0,\quad \frac{\partial w}{\partial r}=0\quad \text{at } r=1, \tag{5a,b}$$

$$\frac{\partial^2 F}{\partial r^2}-\nu\left(\frac{1}{r}\frac{\partial F}{\partial r}+\frac{1}{r^2}\frac{\partial^2 F}{\partial\theta^2}\right)=0\quad \text{at } r=1, \tag{6a}$$

$$\frac{\partial^3 F}{\partial r^3}+\frac{1}{r}\frac{\partial^2 F}{\partial r^2}-\frac{1}{r^2}\frac{\partial F}{\partial r}+\frac{2+\nu}{r^2}\frac{\partial^3 F}{\partial r\partial\theta^2}-\frac{3+\nu}{r^3}\frac{\partial^2 F}{\partial\theta^2}=0\quad \text{at } r=1, \tag{6b}$$

where radius R is assumed to be a non-dimensionalized radius, 1. In addition, it is necessary to require the solution to be bounded at $r=0$.

In order to consider the harmonic excitation we assume the forcing function p as follows:

$$p(r,\theta,t)=\left[\sum_{m=1}^{\infty}P_{0m}\phi_{0m}+2\sum_{n,m=1}^{\infty}P_{nm}\phi_{nm}(r)\cos(n\theta+\tau_{nm})\right]\cos\,\lambda t, \tag{7}$$

where the linear symmetric vibration modes $\phi_{nm}(r)$ correspond to the natural frequencies ω_{nm}, and τ_{nm} denotes phase difference of the excitation, corresponding to the angular displacement θ. In these expressions, the first subscript n refers to the number of nodal diameters, the second subscript m the number of nodal circles including boundary, P_{nm} the coefficients of the forcing, λ the frequency of the harmonic excitation.

3. Steady-state responses

Yeo and Lee [3] considered the case of primary resonance, in which the frequency of excitation λ is near one of the natural frequencies, say, $\omega_{11}=21.2604$. The corresponding mode has one nodal diameter and no other nodal circle but the boundary. They derived a system of autonomous ordinary differential equations with dimension four given as follows:

$$a'=-c_{11}a+\frac{P_{11}}{2\omega_{11}}\sin\,\mu_a, \tag{8a}$$

$$b'=-c_{11}b+\frac{P_{11}}{2\omega_{11}}\sin\,\mu_b, \tag{8b}$$

$$a\mu_a'=\sigma a+\frac{\gamma}{8\omega_{11}}a(a^2+2b^2)+\frac{P_{11}}{2\omega_{11}}\cos\,\mu_a, \tag{8c}$$

$$b\mu_b'=\sigma b+\frac{\gamma}{8\omega_{11}}b(b^2+2a^2)+\frac{P_{11}}{2\omega_{11}}\cos\,\mu_b, \tag{8d}$$

where a, b and μ_a, μ_b denote amplitude and phase variables, respectively, corresponding to the mode with natural frequency ω_{11}. Parameters c_{11}, P_{11} and γ denote damping coefficient, excitation amplitude, and nonlinear coefficient, respectively, corresponding to the mode. The external detuning parameter σ is defined by $\lambda = \omega_{11} + \hat{\sigma}$ and $\hat{\sigma} = \varepsilon\sigma$. It is worthwhile to note that system (1) is invariant under the interchanges of variables such as $a \leftrightarrow b$ and $\mu_a \leftrightarrow \mu_b$. Since our main concern is steady-state responses of the plate, first of all, we consider equilibrium solutions ($a' = b' = \mu_a' = \mu_b' = 0$), each of which corresponds to a steady-state response. We can write the steady-state response to the first-order approximation as

$$w = \phi_{11}\{a\cos(\lambda t - \mu_a + \theta + \tau) + b\cos(\lambda t - \mu_b - \theta - \tau)\}, \tag{9}$$

where the response w is a superposition of the two traveling waves rotating clockwise and counterclockwise, respectively, and τ is a phase difference corresponding to θ. When $a = b$ and $\mu_a = \mu_b$, form (9) is reduced to a standing wave as follows:

$$w = 2\phi_{11}a\cos(\lambda t - \mu_a)\cos(\theta + \tau). \tag{10}$$

4. Stability and basin boundaries

4.1. Steady-state responses and their stability

Yeo and Lee [3] plotted Fig. 2 to show the amplitudes a, b of equilibrium solutions of system (4) as functions of detuning parameter $\varepsilon\sigma = \hat{\sigma}$ when $\{\nu, \varepsilon, \varepsilon c_{11}, \varepsilon P_{11}, \gamma\} = \{1/3, 0.001067, 0.01, 4, -772.04\}$. Solid and dotted lines denote, respectively, stable (S: the first abbreviation) and unstable (U) responses. Branches SS1, US1, SS2 and US2 represent standing (S: the second abbreviation) waves ($a = b$), while ST1, UT1 and UT2 represent traveling (T) waves ($a \neq b$). The figure shows that the response curve corresponding to standing waves is similar with the response curve of the Duffing oscillator, except that the branch SS1 changes its stability at pitchfork bifurcation point $\hat{\sigma}_A$ (0.0245). Reminding the invariance of the system, we can see that there exist two stable traveling waves (denoted by ST1) bifurcated at the point. One (ST1-1: $a > b$) is rotating clockwise and the other (ST1-2: $a < b$) rotating counter-clockwise. We believe that a close investigation into regions Z1, Z2, and Z3 is needed. All responses in these regions look unstable, which is a remarkable contrary to the saddle-node bifurcation.

Enlargements of regions Z1, Z2 and Z3 in Fig. 2 are shown in Fig. 3(a), (b) and (c), respectively. More stable branches ST2 and SS1 are some rewards of the close investigation. The branch ST2 representing stable traveling wave changes its stability at Hopf bifurcation points, $\hat{\sigma}_D$ (0.13264) and $\hat{\sigma}_F$ (1.28484). The branch SS1 representing stable standing wave regains its stability at pitchfork bifurcation points, $\hat{\sigma}_G$ (1.28554). These figures show that the response curves have four saddle-node bifurcation points, $\hat{\sigma}_B$ (0.0950), $\hat{\sigma}_C$ (0.13248),

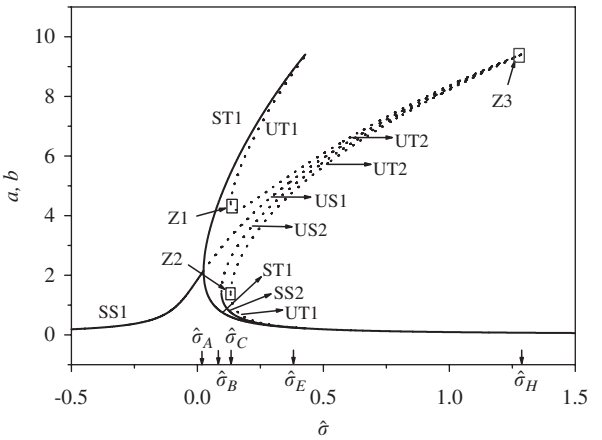

Fig. 2. Variations of the amplitudes with detuning parameter $\hat{\sigma} = \varepsilon\sigma$. —, stable; · · · · · · , unstable [3].

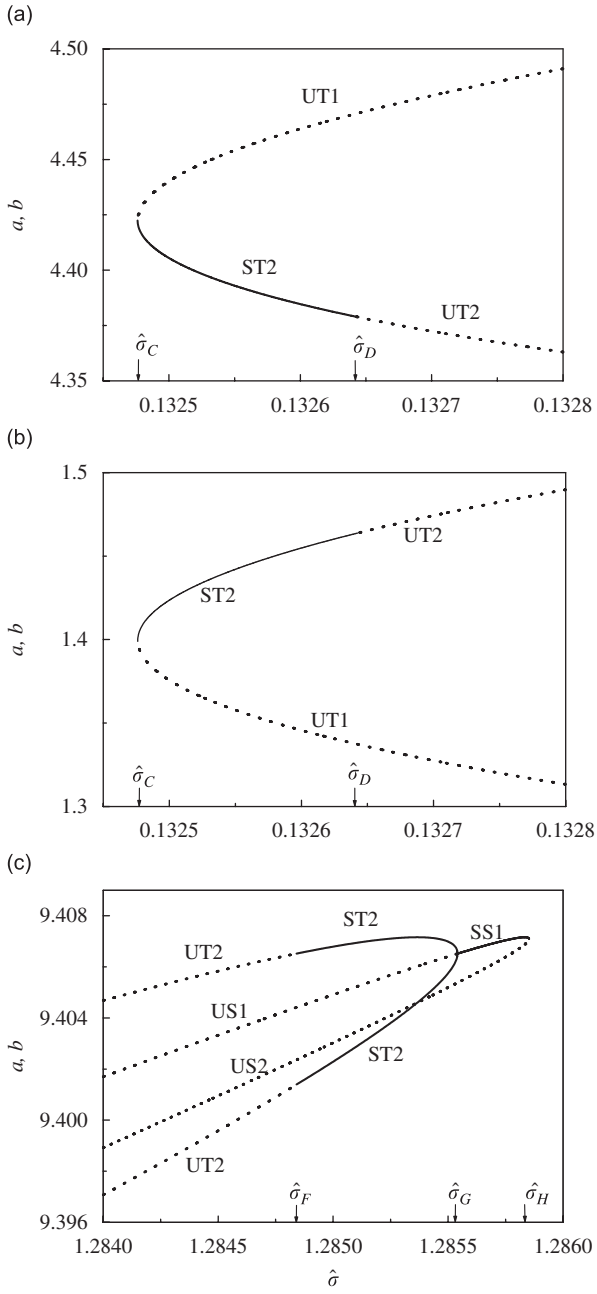

Fig. 3. Variations of the amplitudes with detuning parameter $\hat{\sigma} = \varepsilon\sigma$: —, stable; · · · · · · , unstable. Enlargements of the Z1, Z2, Z3 in Fig. 2. (a) Z1, (b) Z2 and (c) Z3.

$\hat{\sigma}_E$ (0.42902) and $\hat{\sigma}_H$ (1.28586). When $\hat{\sigma}_C < \hat{\sigma} < \hat{\sigma}_D$, there exist five stable steady-state responses, SS2, ST1-1 (clockwise), ST1-2 (counter-clockwise), ST2-1 (clockwise) and ST2-2 (counter-clockwise). The initial condition determines which deflection is to be realized.

4.2. Chaotic motions

In view of Hopf bifurcations at $\hat{\sigma}_D$ and $\hat{\sigma}_F$, we can see that when $\hat{\sigma}_D < \hat{\sigma} < \hat{\sigma}_F$, the unstable branches UT2 of Fig. 3 generate periodic solutions of system (8). The periodicity of amplitude and phase variables implies that

each component of response (9) becomes aperiodic. In consequence this aperiodicity of components results in amplitude- and phase-modulated motions of the plate. In order to examine the behavior of the periodic solutions of system (8) we construct the Poincaré map by using a hyperplane, $\mu_a = -0.12a + 3.1834$.

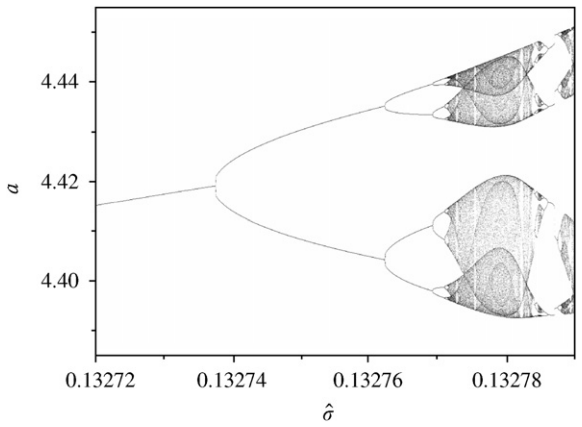

Fig. 4. Bifurcation diagram for the Poincaré map of the steady-state solutions generated from UT2.

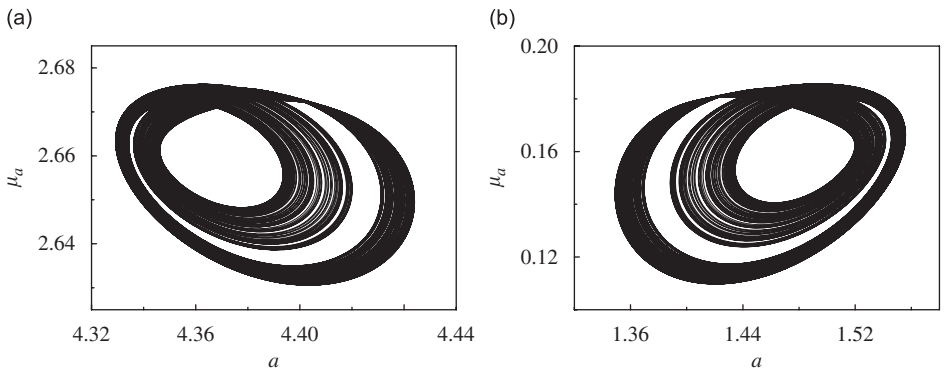

Fig. 5. Phase plots for chaotic solutions at detuning parameter $\hat{\sigma} = 0.132777$: (a) $a > b$ and (b) $a < b$.

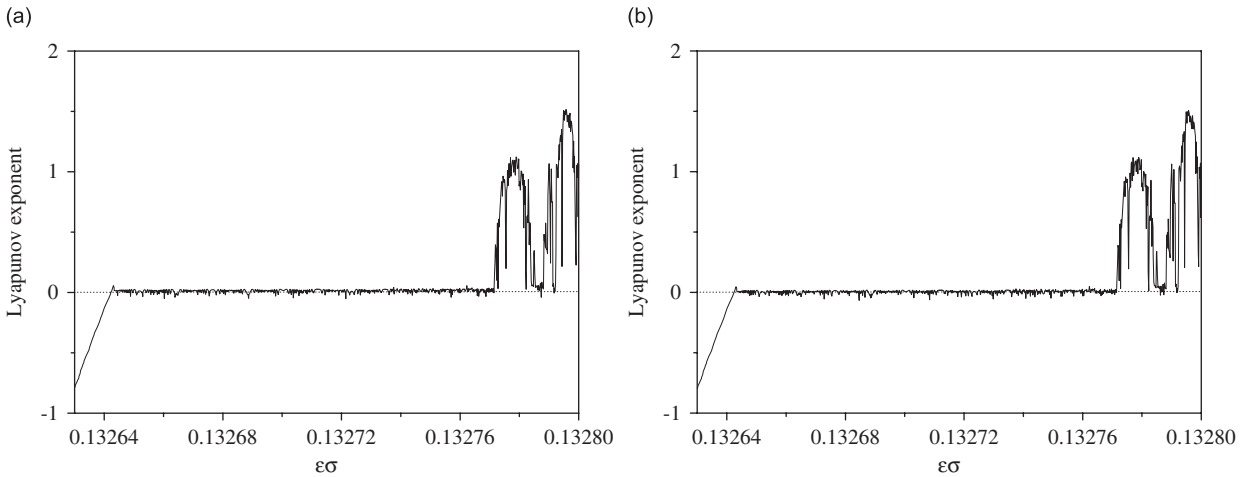

Fig. 6. Lyapunov exponent versus detuning parameter $\hat{\sigma}$: (a) $a > b$ and (b) $a < b$.

The bifurcation diagram in Fig. 4 shows the relation between $\hat{\sigma}$ and a of periodic solutions in the map. The diagram also shows the period-doubling bifurcation leading to the chaotic motions as in Refs. [13,14]. The phase trajectories of chaotic motions at detuning parameter $\hat{\sigma} = 0.132777$, representing modulated traveling waves rotating clockwise (generated from UT2-1) and counter-clockwise (generated from UT2-2), are shown in Fig. 5(a) and (b), respectively. In order to show quantitatively that the motions shown in Fig. 5(a) and (b) are truly chaotic, we calculated the largest Lyapunov exponents of long-term responses for system (8).

Table 1
Equilibrium solutions for different $\hat{\sigma}$ values

$\hat{\sigma}$	$\mathbf{x}_i$	x_1	x_2	x_3	x_4
0.132643 (P-1)	$\mathbf{x}_1$	−0.7514337	0.0604117	−0.7514337	0.0604117
	$\mathbf{x}_{2(1)}$	−3.8755831	2.0383368	1.4460590	0.2278031
	$\mathbf{x}_{2(2)}$	1.4460590	0.2278031	−3.8755831	2.0383368
0.132752 (P-2)	$\mathbf{x}_1$	−0.7506858	0.0602907	−0.7506858	0.0602907
	$\mathbf{x}_{2(1)}$	−3.8681330	2.0275357	1.4641592	0.2336915
	$\mathbf{x}_{2(2)}$	1.4641592	0.2336915	−3.8681330	2.0275357
0.132765 (P-4)	$\mathbf{x}_1$	−0.7505968	0.0602764	−0.7505968	0.0602764
	$\mathbf{x}_{2(1)}$	−3.8673651	2.0264260	1.4660641	0.2343160
	$\mathbf{x}_{2(2)}$	1.4660641	0.2343160	−3.8673651	2.0264260
0.132771 (P-8)	$\mathbf{x}_1$	−0.7505557	0.0602696	−0.7505557	0.0602696
	$\mathbf{x}_{2(1)}$	−3.8670172	2.0259236	1.4669295	0.2346000
	$\mathbf{x}_{2(2)}$	1.4669295	0.2346000	−3.8670172	2.0259236
0.1327711 (P-16)	$\mathbf{x}_1$	−0.7505550	0.0602696	−0.7505550	0.0602696
	$\mathbf{x}_{2(1)}$	−3.8670115	2.0259153	1.4669439	0.2346047
	$\mathbf{x}_{2(2)}$	1.4669439	0.2346047	−3.8670115	2.0259153
0.1327713 (P-32)	$\mathbf{x}_1$	−0.7505536	0.0602693	−0.7505536	0.0602693
	$\mathbf{x}_{2(1)}$	−3.8670000	2.0258986	1.4669726	0.2346141
	$\mathbf{x}_{2(2)}$	0.2346141	1.4669726	−3.8670000	2.0258986
0.132777 (P-∞)	$\mathbf{x}_1$	−0.7504939	0.0060260	−0.7504939	0.0060260
	$\mathbf{x}_{2(1)}$	−3.8665029	2.0251810	1.4682119	0.2350211
	$\mathbf{x}_{2(2)}$	1.4682119	0.2350211	−3.8665029	2.0251810

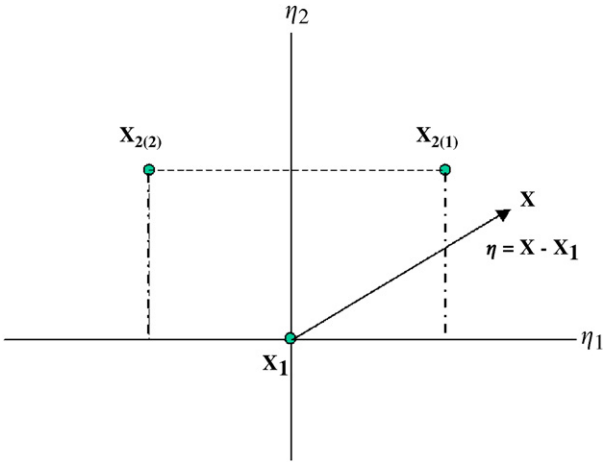

Fig. 7. New Cartesian coordinates, η_1 and η_2, on the principal plane.

The results are shown in Fig. 6(a) and (b), respectively, corresponding to attractors in the cases of $a>b$ and $a<b$. In principle, a response is chaotic if the exponent is positive. The figure tells not only that the largest Lyapunov exponent corresponding to each attractor ($\hat{\sigma} = 0.132777$) in Fig. 5(a) and (b) has a positive value, 1.1173, but also that the region of positive exponent agrees with the region of aperiodic motions in Fig. 4.

4.3. Basin boundary for the chaotic motions

It is found that there exist at most five stable responses: one standing wave and four traveling waves. Two of traveling waves lose their stability by Hopf bifurcations and experience a sequence of period-doubling

Table 2
Unit vectors defining the principal plane for detuning parameter

$\hat{\sigma}$	$\mathbf{u}_i$	u_{i1}	u_{i2}	u_{i3}	u_{i4}
0.132643 (P-1)	$\mathbf{u}_1$	−0.7514337	0.0604117	−0.7514337	0.0604117
	$\mathbf{u}_2$	−3.8755831	−2.0383368	1.4460590	0.2278031
0.132752 (P-2)	$\mathbf{u}_1$	−0.6701989	0.2254626	0.6701989	−0.2254626
	$\mathbf{u}_2$	−0.2747280	0.6515555	−0.2747280	0.6515555
0.132765 (P-4)	$\mathbf{u}_1$	−0.6702793	0.2252236	0.6702793	−0.2252236
	$\mathbf{u}_2$	−0.2741326	0.6518062	−0.2741326	0.6518062
0.132771 (P-8)	$\mathbf{u}_1$	−0.6703157	0.2251152	0.6703157	−0.2251152
	$\mathbf{u}_2$	−0.2738621	0.6519200	−0.2738621	0.6519200
0.1327711 (P-16)	$\mathbf{u}_1$	−0.6703163	0.2251134	0.6703163	−0.2251134
	$\mathbf{u}_2$	−0.2738576	0.6519218	−0.2738576	−0.2251134
0.1327713 (P-32)	$\mathbf{u}_1$	−0.6703175	0.2251098	0.6703175	−0.2251098
	$\mathbf{u}_2$	−0.2738487	0.6519255	−0.2738487	0.6519255
0.132777 (P-∞)	$\mathbf{u}_1$	−0.6703696	0.2249546	0.6703696	−0.2249546
	$\mathbf{u}_2$	−0.2734615	0.6520881	−0.2734615	0.6520881

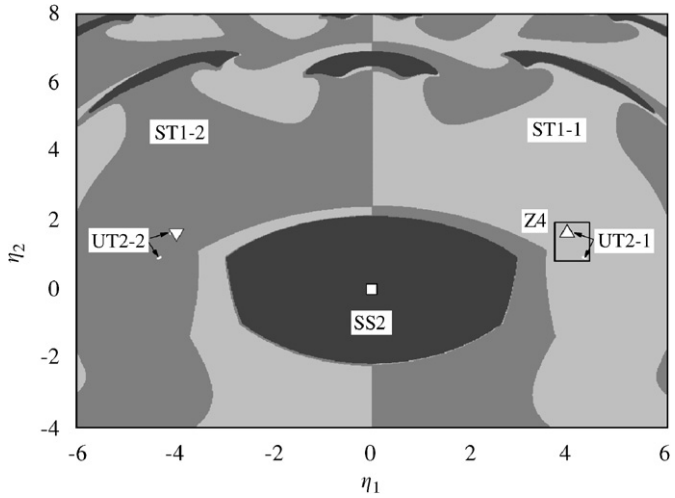

Fig. 8. The basins of attraction in the principal plane for detuning parameter, $\hat{\sigma} = 0.132777$: □, the stable equilibrium solution SS2; △, the unstable equilibrium solution UT2-1; ▽, the unstable equilibrium solution UT2-2. The black, dark gray and gray basins are attracted to SS2, ST1-1 and ST1-2, respectively. The white basins at the right (in Z4) and the left are attracted to chaotic motions generated from UT2-1 and UT2-2, respectively.

bifurcations leading to chaos. We consider the case of $\{v, \varepsilon, \varepsilon c, \varepsilon\sigma, \varepsilon P_{11}, \gamma\} = \{\frac{1}{3}, 0.001067, 0.01, 0.132777, 4, -772.046\}$, when the system has five attractors: three equilibrium solutions (one standing wave and two traveling waves) and two chaotic attractors (modulated traveling waves). Then the asymptotic behavior of the system depends on the initial condition. A set of initial states, a basin of attraction, is attracted to one of attractors.

Having difficulty in representing graphically the basins of attraction in a four-dimensional space, we use the concept of the principal plane [15]. This two-dimensional plane includes three equilibrium points (listed in Table 1) of the system corresponding to one stable standing wave (SS2) and two unstable traveling waves (UT2-1 and UT2-2). From Table 1, noting that two equilibrium solutions, UT2-1 and UT2-2 are located at the equal distances from SS2 solution, we establish a Cartesian coordinate system η_1, η_2 on the principal plane, so that the SS2 solution is at the origin and two equilibrium solutions, UT2-1 and UT2-2 are at equal distances from the η_2 axes, as shown in Fig. 7. Let $\mathbf{u}_1$ and $\mathbf{u}_2$ be unit vectors along the η_1 and η_2 axes, respectively. Then the principal plane can be defined by these unit vectors:

$$\mathbf{u}_1 = \frac{\mathbf{x}_{2(1)} - \mathbf{x}_{2(2)}}{|\mathbf{x}_{2(1)} - \mathbf{x}_{2(2)}|}, \quad \mathbf{u}_2 = \frac{\mathbf{x}_{2(1)} + \mathbf{x}_{2(2)} - 2\mathbf{x}_1}{|\mathbf{x}_{2(1)} + \mathbf{x}_{2(2)} - 2\mathbf{x}_1|}, \tag{11}$$

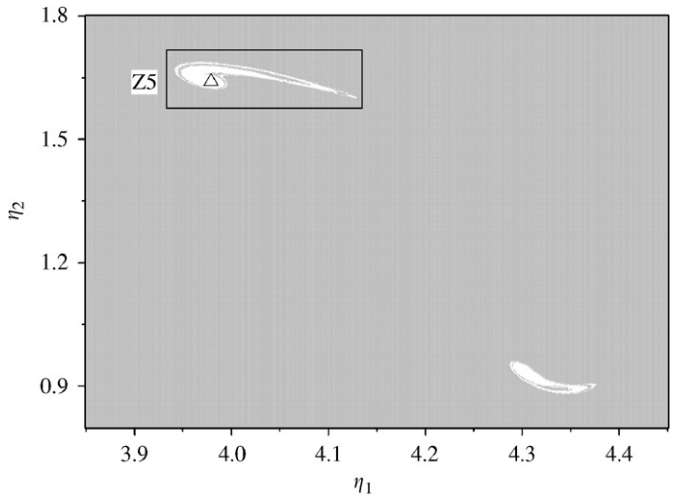

Fig. 9. The basins of attraction in the principal plane for detuning parameter, $\hat{\sigma} = 0.132777$. Enlargement of Z4 in Fig. 8; △, the unstable equilibrium solution UT2-1. The gray and white basins are attracted to ST1-1 and chaotic motion generated from UT2-1, respectively.

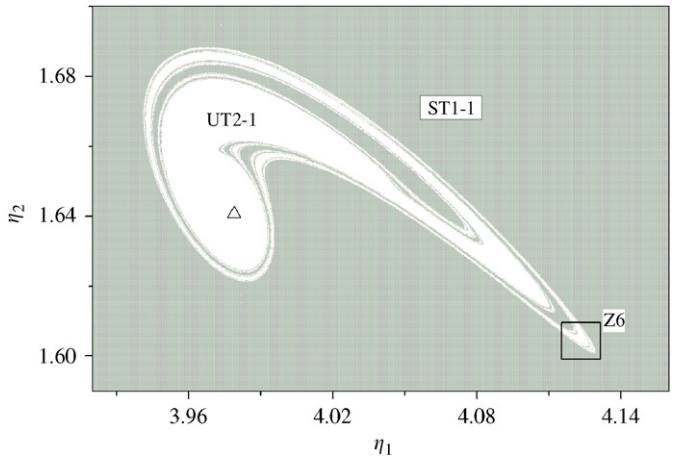

Fig. 10. The basins of attraction in the principal plane for detuning parameter, $\hat{\sigma} = 0.132777$. Enlargement of Z5 in Fig. 9; △, the unstable equilibrium solution UT2-1. The gray and white basins are attracted to ST1-1 and chaotic motion generated from UT2-1, respectively.

where $\mathbf{x}_1$, $\mathbf{x}_{2(1)}$ and $\mathbf{x}_{2(2)}$ denotes SS2 , UT2-1 and UT2-2, respectively. Unit vectors defining the principal plane are given in Table 2, where

$$\mathbf{u}_i = \sum_{j=1}^{4} u_{ij}\mathbf{e}_j. \tag{12}$$

It should be noted that the principal plane varies with $\hat{\sigma}$. In Tables 1 and 2 are listed the data for not only the case of $\hat{\sigma} = 0.132777$ but also some other cases for the later reference. A point $\mathbf{x}$ in the plane can be expressed as

$$\mathbf{x} = \mathbf{x}_1 + \boldsymbol{\eta} = \mathbf{x}_1 + \sum_{i=1}^{2} \eta_i \mathbf{u}_i. \tag{13}$$

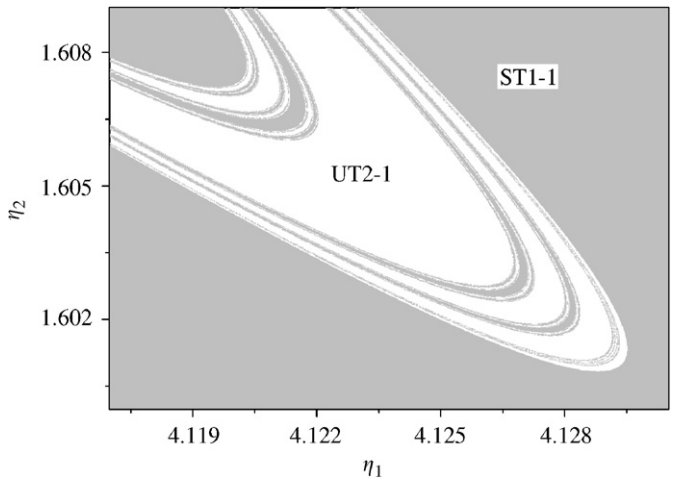

Fig. 11. The basins of attraction in the principal plane for detuning parameter, $\hat{\sigma} = 0.132777$. Enlargement of Z6 in Fig. 10. The gray and white basins are attracted to ST1-1 and chaotic motion generated from UT2-1, respectively.

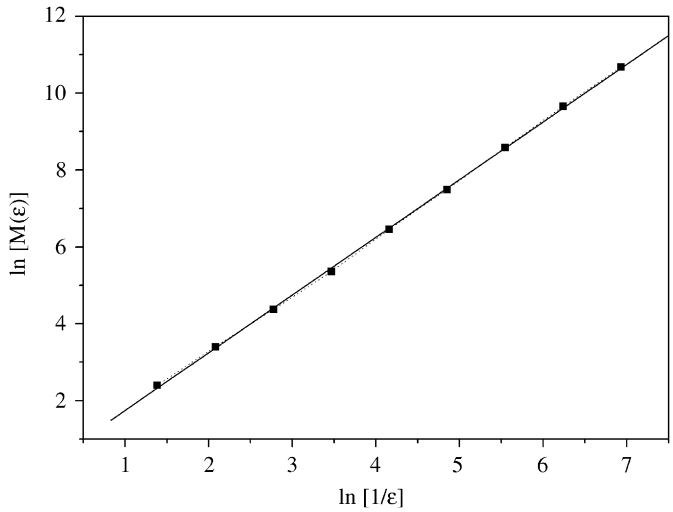

Fig. 12. Log–log diagram for measurement of the box-counting dimension of the fractal basin boundary. The dimension is 1.537 noted as the slope of the linear regression line.

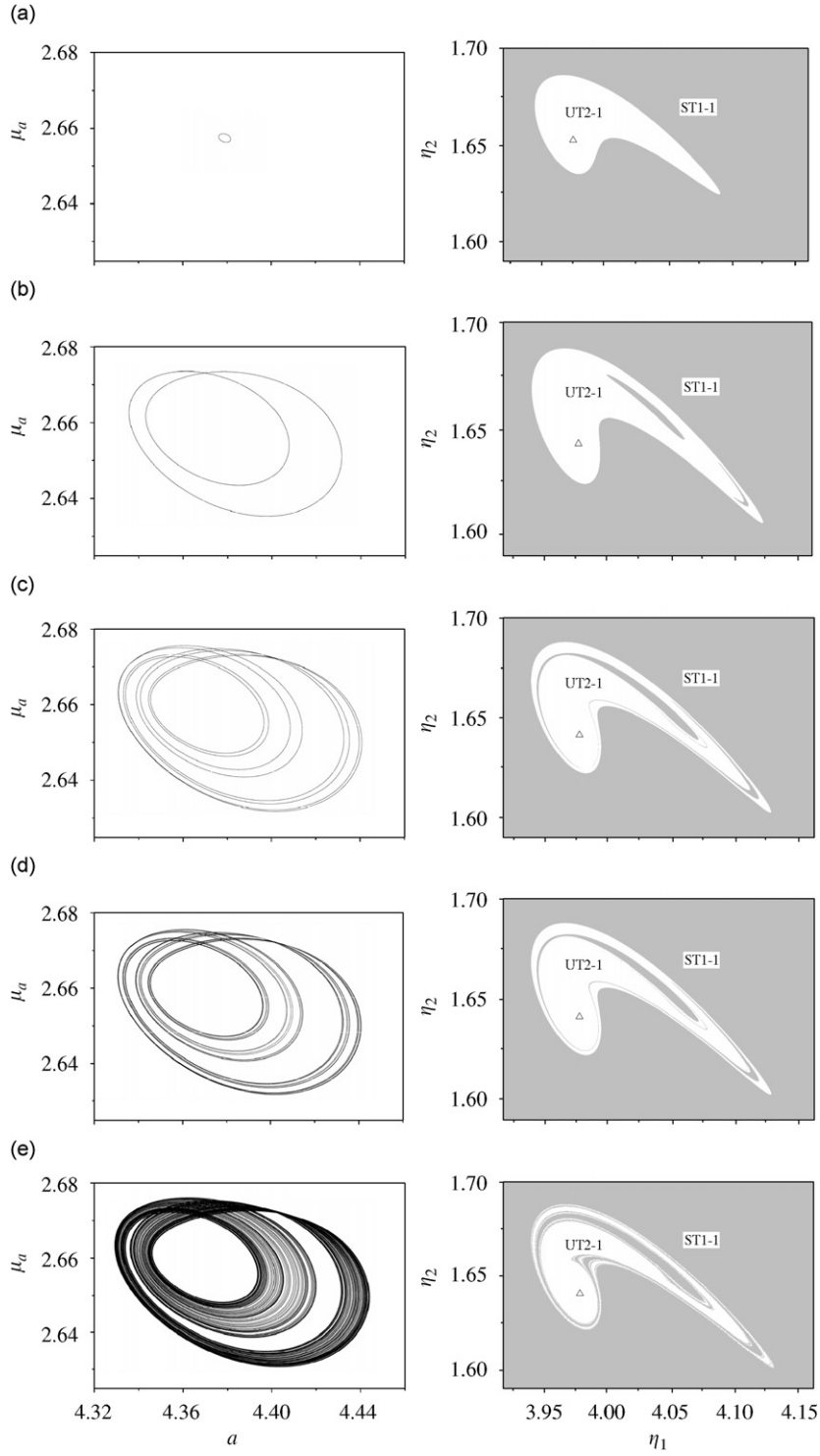

Fig. 13. Phase trajectories and basin boundaries of modulated motions in a period-doubling sequence. (a) $\varepsilon\sigma = 0.132643$(period-1, fractal dimension = 1.049). (b) $\varepsilon\sigma = 0.132752$(period-2, fractal dimension = 1.135). (c) $\varepsilon\sigma = 0.132771$(period-8, fractal dimension = 1.303). (d) $\varepsilon\sigma = 0.1327713$(period-32, fractal dimension = 1.327). (e) $\varepsilon\sigma = 0.132777$(period-$\infty$, fractal dimension = 1.537). The grey and white basins are attracted to ST1-1 and modulated motions generated from UT2-1, respectively.

The equilibrium points SS2, UT2-1 and UT2-2 are denoted by a square (□), an upward triangle (△) and a downward triangle (▽), respectively, in Fig. 8. The figure shows five basins of attraction represented by SS2 (black), UT2-1 (white in the right), UT2-2 (white in the left), and two traveling waves ST1-1 (gray), ST1-2 (dark gray), each of which is attracted to each of five attractors. In order to examine more closely the basin of attraction of chaotic motion (UT2-1), we enlarge region Z4 to obtain Fig. 9. Consecutively enlarged results are shown in Figs. 10 and 11, from which we can see that the basin boundary of the chaotic motion has the unlimited number of lines with self-similarity. This is the fractal nature of the basin boundary. The long-term response of the plate varies even with small change of initial condition in this boundary.

In order to measure quantitative characterization of the geometrical structure of the boundary, we need to determine its fractal dimension. Among several kinds of the dimensions, the box-counting dimension is calculated in this study. We cover the space in the principal plane, including the boundary, by a grid of squares of edge length ε_o. We then count the number of squares $M(\varepsilon_o)$ needed to cover the boundary. The box-counting dimension [16–19] d is given by

$$d = \lim_{\varepsilon_o \to 0} \frac{\ln M(\varepsilon_o)}{\ln(1/\varepsilon_o)}. \tag{14}$$

The dimension d is represented by the slope of the straight solid line in Fig. 12 showing the log–log diagram. The basin boundary of the chaotic motion on the principal plane is shown to have a fractal dimension of 1.537.

4.4. Evolution of basin boundaries of modulated motions

In the previous section, for the case of $\{\varepsilon, \omega_{11}, \varepsilon c_{11}, \varepsilon P_{11}, \gamma\} = \{0.001067, 21.2604, 0.01, 4, -772.046\}$, it was found that system (1) experiences Hopf bifurcation at $\varepsilon\sigma = 0.132643$, at which two of traveling waves lose their stability. A sequence of period-doubling bifurcations leads to chaos when $\varepsilon\sigma = 0.132777$. When $\varepsilon\sigma$ is between these values, the system has five attractors: three equilibrium solutions (three periodic waves: one standing wave and two traveling waves) and two modulated motions (two quasi-periodic traveling waves). We examine how the basin boundaries evolve as $\varepsilon\sigma$ varies. We also calculate the box counting dimensions [19] of the basin boundaries. By means of Tables 1 and 2, the results are shown in Fig. 13. Phase trajectories and basin boundaries corresponding to the different values of $\varepsilon\sigma$ are shown in the left- and right-hand sides of the figure, respectively. The white (UT2-1) and gray (ST1-1) regions in the right-hand side of the figure represent domains of attraction of non-periodic and periodic traveling waves, respectively, where both types of traveling waves are rotating clockwise. Examining the evolution and fractal dimensions of basin boundaries, we can observe that the basin boundaries of the modulated motions turn out to have the fractal nature.

5. Conclusions

In order to investigate further nonlinear asymmetric vibrations of a clamped circular plate under a harmonic excitation, we reexamine a primary resonance ($\lambda \approx \omega_{11}$), studied by Yeo and Lee [3] in which at most three stable steady-state responses (one standing wave and two traveling waves) are observed to exist. Further examination, however, tells that there exist at most five stable steady-state responses: one standing wave and four traveling waves. Two of the traveling waves lose their stability by Hopf bifurcation and have a sequence of period-doubling bifurcations leading to chaos. When the system has five attractors: three equilibrium solutions (one standing wave and two traveling waves) and two chaotic attractors (two modulated traveling waves), the basin boundaries of the attractors on the principal plane are obtained. Also examined is how basin boundaries of the modulated motions (quasi-periodic and chaotic motions) evolve as a system parameter varies. The basin boundaries of the modulated motions turn out to have the fractal nature.

References

[1] G.J. Efstathiades, A new approach to the large-deflection vibrations of imperfect circular disks using Galerkin's procedure, *Journal of Sound and Vibration* 16 (1971) 231–253.

[2] S. Sridhar, D.T. Mook, A.H. Nayfeh, Non-linear resonances in the forced responses of plates, Part II: asymmetric responses of circular plates, *Journal of Sound and Vibration* 59 (1978) 159–170.
[3] M.H. Yeo, W.K. Lee, Corrected solvability conditions for non-linear asymmetric vibrations of a circular plate, *Journal of Sound and Vibration* 257 (2002) 653–665.
[4] W.K. Lee, M.H. Yeo, Non-linear interactions in asymmetric vibrations of a circular plate, *Journal of Sound and Vibration* 263 (2003) 1017–1030.
[5] W.K. Lee, M.H. Yeo, S.B. Samoilenko, The effect of the number of nodal diameters on non-linear interactions in two asymmetric vibration modes of a circular plate, *Journal of Sound and Vibration* 268 (2003) 1013–1023.
[6] W.K. Lee, Modal interactions in asymmetric vibrations of circular plates, in: J.-Q. Sun, A.C.J. Luo (Eds.), *Advances in Nonlinear Science and Complexity, Vol. 1: Bifurcation and Chaos in Complex Systems*, Elsevier, Amsterdam, 2006.
[7] M.H. Yeo, W.K. Lee, Evidences of global bifurcations of an imperfect circular plate, *Journal of Sound and Vibration* 293 (2006) 138–155.
[8] S.B. Samoylenko, W.K. Lee, Global bifurcations and chaos in a harmonically excited and undamped circular plate, *Nonlinear Dynamics* 47 (2007) 405–419.
[9] C. Touzé, O. Thomas, A. Chaigne, Asymmetric non-linear forced vibrations of free-edge circular plates. Part I: theory, *Journal of Sound and Vibration* 258 (2002) 649–676.
[10] O. Thomas, C. Touzé, A. Chaigne, Asymmetric non-linear forced vibrations of free-edge circular plates. Part II: experiments, *Journal of Sound and Vibration* 265 (2003) 1075–1101.
[11] S. Sridhar, D.T. Mook, A.H. Nayfeh, Non-linear resonances in the forced responses of plates. Part I: symmetric responses of circular plates, *Journal of Sound and Vibration* 41 (1975) 359–373.
[12] A.H. Nayfeh, D.T. Mook, *Nonlinear Oscillations*, Wiley, New York, 1979.
[13] W.K. Lee, H.D. Park, Chaotic dynamics of a harmonically excited spring-pendulum system with internal resonance, *Nonlinear Dynamics* 14 (3) (1997) 211–229.
[14] W.K. Lee, H.D. Park, Second-order approximation for chaotic responses of a harmonically excited spring-pendulum system, *International Journal of Nonlinear Mechanics* 34 (4) (1999) 749–757.
[15] W.K. Lee, C.S. Hsu, A global analysis of an harmonically excited spring-pendulum system with internal resonance, *Journal of Sound and Vibration* 171 (1994) 335–359.
[16] A.J. Lichtenberg, M.A. Lieberman, *Regular and Stochastic Motion*, Springer, New York, 1983.
[17] C. Grebogi, S.W. Mcdonald, E. Ott, J.A. Yorke, Final state sensitivity: an obstruction to predictability, *Physics Letters* 99A (9) (1983) 415–418.
[18] H.O. Peitgen, H. Jürgens, D. Saupe, *Chaos and Fractals: New Frontiers of Science*, Springer, New York, 1992.
[19] E. Ott, *Chaos in Dynamical Systems*, Cambridge University Press, Cambridge, 1993.